Unraveling the Microstructure-Related Device Stability for Polymer Solar Cells Based on Nonfullerene Small-Molecular Acceptors

Xiaoyan Du, Thomas Heumueller, Wolfgang Gruber, Osbel Almora, Andrej Classen, Jianfei Qu, Feng He, Tobias Unruh, Ning Li,* and Christoph J. Brabec*

As the power conversion efficiency (PCE) of organic solar cells (OSCs) has surpassed the 17% baseline, the long-term stability of highly efficient OSCs is essential for the practical application of this photovoltaic technology. Here, the photostability and possible degradation mechanisms of three state-of-the-art polymer donors with a commonly used nonfullerene acceptor (NFA), IT-4F, are investigated. The active-layer materials show excellent intrinsic photostability. The initial morphology, in particular the mixed region, causes degradation predominantly in the fill factor (FF) under illumination. Electron traps are formed due to the reorganization of polymers and diffusion-limited aggregation of NFAs to assemble small isolated acceptor domains under illumination. These electron traps lead to losses mainly in FF, which is in contradistinction to the degradation mechanisms observed for fullerene-based OSCs. Control of the composition of NFAs close to the thermodynamic equilibrium limit while keeping adequate electron percolation and improving the initial polymer and NFA ordering are of the essence to stabilize the FF in NFA-based solar cells, which may be the key tactics to develop next-generation OSCs with high efficiency as well as excellent stability.

The power conversion efficiency (PCE) of organic solar cells (OSCs) has been significantly improved with the development of nonfullerene acceptors (NFAs).[1] Certificated PCE of over 17% has been reported.[2] Long-term photostability is critical for commercialization of this photovoltaic technology. However, understanding of degradation mechanisms is much lagging behind the PCE thriving. Identification of degradation mechanisms will definitely contribute to materials design rules for highly efficient and stable OSCs.[3–5]

Compared to extrinsic instabilities, e.g., chemical reaction with oxygen (with or without light)[6] and water,[7] the intrinsic materials stability against light and the microstructure changes upon external stress are most relevant in the phase of new materials development. Most of the stability studies so far have been focused on fullerene-based OSCs,[7–10] while for

Dr. X. Du, Dr. T. Heumueller, O. Almora, A. Classen,
Dr. N. Li, Prof. C. J. Brabec
Institute of Materials for Electronics and Energy Technology (i-MEET)
Department of Materials Science and Engineering
Friedrich-Alexander-Universität Erlangen-Nürnberg
Martensstrasse 7, 91058 Erlangen, Germany
E-mail: ning.li@fau.de; christoph.brabec@fau.de
Dr. X. Du, Dr. T. Heumueller, A. Classen, Dr. N. Li, Prof. C. J. Brabec
Helmholtz-Institute Erlangen-Nürnberg (HI ERN)
Immerwahrstrasse 2, 91058 Erlangen, Germany
Dr. W. Gruber, Prof. T. Unruh
Institute of Crystallography and Structural Physics
Department of Physics
Friedrich-Alexander-Universität Erlangen-Nürnberg
Staudtstr. 3, 91058 Erlangen, Germany

Dr. W. Gruber, Prof. T. Unruh
Center for Nanoanalysis and Electron Microscopy (CENEM)
Interdisciplinary Center for Nanostructured Films (IZNF)
Friedrich-Alexander-Universität Erlangen-Nürnberg (FAU)
Cauerstr. 3, 91058 Erlangen, Germany
O. Almora
Erlangen Graduate School in Advanced Optical Technologies (SAOT)
Friedrich-Alexander-Universität Erlangen-Nürnberg
91052 Erlangen, Germany
J. Qu, Prof. F. He
Shenzhen Grubbs Institute and Department of Chemistry
Southern University of Science and Technology
Shenzhen 518055, China
Dr. N. Li
National Engineering Research Center for Advanced Polymer
Processing Technology
Zhengzhou University
No. 100 Science Avenue 450002, Zhengzhou, P. R. China

unstable NFA-based OSCs, understanding of the degradation mechanism is still limited. For NFA-based systems, promising photostability has been demonstrated for many-systems including P3HT:IDTBR,[11] PCE10 with EH-IDTBR,[12] or IEICO-4F,[13] PffBT4T-2OD:EH-IDTBR,[14] single-component devices[15] as well as ITIC derivatives.[4,16] However, studies up to date indicated that the light stability of NFA systems is strongly materials-dependent.[4,17] As a general trend, degradation of NFA systems is different compared to those based on fullerene derivatives. For example, J_{SC} degradation as a result of materials incompatibility[8,9,18–20] or fullerene dimerization[21,22] has been revealed for several polymer:phenyl-C_{61}-butyric acid methyl ester (PCBM) combinations. Open circuit voltage (V_{OC}) losses are observed which is related to density of states broadening at the donor and acceptor interface and depend much on polymer crystallinity.[23,24] In strong contrast, fill factor (FF) degradation dominated the losses in several of the reported degradation of NFA-based systems, while V_{OC} and J_{SC} maintained almost unchanged during the degradation process.[11,25] The mechanism behind is yet to be elucidated.

Previously we have shown that photostability of OSCs based on PBDB-T and a series of ITIC derivatives significantly depends on the NFA molecular engineering on side chains and end groups.[4] Most importantly, devices based on poly[[(2,6-(4,8-bis(5-(2-ethylhexyl)thiophen-2-yl)-benzo[1,2-b:4,5-b']dithiophene))-*alt*-(5,5-(1',3'-di-2-thienyl-5',7'-bis(2-ethylhexyl)benzo[1',2'-c:4',5'-c']dithiophene-4,8-dione))]] (PBDB-T) as polymer donor (D) and 3,9-bis(2-methylene-((3-(1,1-dicyanomethylene)-6,7-difluoro)-indanone))-5,5,11,11-tetrakis(4-hexylphenyl)-dithieno[2,3-d:2',3'-d']-s-indaceno[1,2-b:5,6-b']dithiophene (IT-4F) (previously

termed as ITIC-2F) as electron acceptor (A) showed the best light stability after a burn-in loss in FF with an extrapolated T_{80} lifetime (80% of the initial PCE) reaching 11 000 h. However, due to energy level mismatch of the PBDB-T with IT-4F, device performance was low (≈8%). Fluorination and chlorination of the thiophene unit of the benzodithiophene (BDT) side chains leads to PBDB-T-2F (PM6) and PBDB-T-2Cl (PM7) with deeper lying frontier molecular orbitals and increased PCE > 13%.[26,27]

In this work, we investigate photostability of OSCs incorporating fluorinated (PM6) and chlorinated (PM7) polymer donors and IT-4F as an acceptor under the same condition as previously reported[4] (i.e., under inert atmosphere and white light-emitting diode (LED) illumination). Similar to many other NFA-based material systems but different from fullerene-based OSCs, the degradation is dominated by FF loss, which is attributed to the formation of local isolated NFA aggregates in the mixed region due to materials incompatibility and diffusion-limited aggregation of IT-4F. It is evidenced that increasing molecular ordering using either solvent additives or thermal stress on the active layer can effectively improve the morphological stability of these IT-4F-based OSCs under illumination.

Figure 1 shows the chemical structure of polymer donors (PBDB-T, PM6, and PM7) and IT-4F investigated in this work. By replacing PBDB-T with PM6 or PM7, both J_{SC} and V_{OC} of OSCs could be significantly improved, as shown in Figure 1b; and Table S1 (Supporting Information). We demonstrated previously that the stability of photoactive materials could be fast and reliably analyzed by measuring space-charge-limited current of hole-only or electron-only devices under illumination.[4]
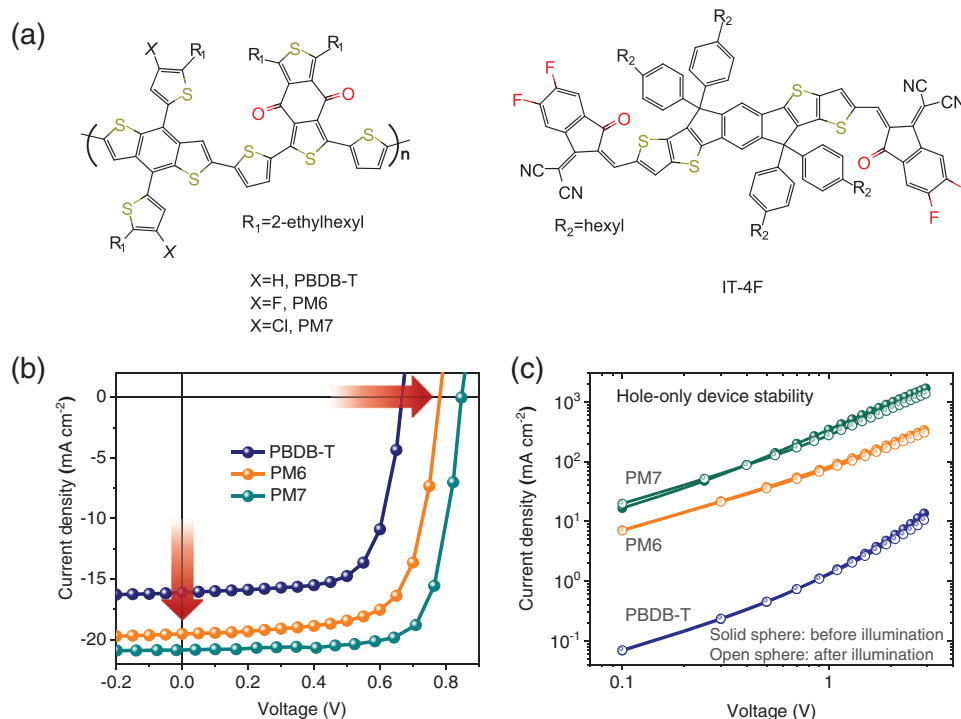
Figure 1. a) Chemical structure of PBDB-T, PM6, PM7, and IT-4F used in this work. b) Current density–voltage characteristics of solar cells based on different polymers blended with IT-4F in inverted structure. c) Photostability of hole-only devices based on the investigated polymer materials aged under white LED illumination for 70 h.
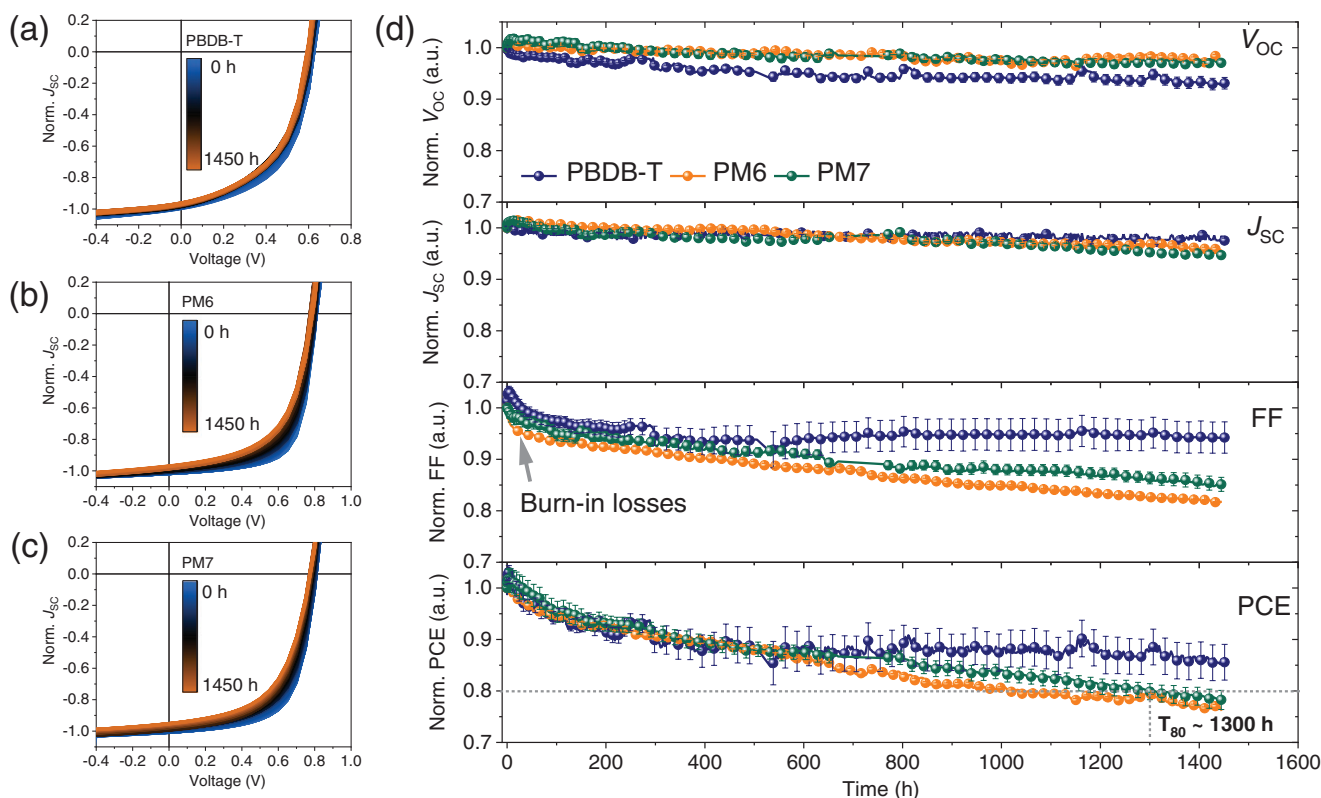
Figure 2. Photostability of devices based on PBDB-T, PM6, and PM7 blended with IT-4F in a weight ratio of 1:1 under continuous LED illumination and room temperature. a–c) Recorded current–voltage curves (with normalized initial short-circuit current density) and d) photovoltaics parameters (averaged over 6 devices) as a function of time for devices based on different photoactive layers as indicated in the legend. T_{80} (80% of the initial PCE) lifetime for PM6- and PM7-based solar cells are indicated.

The stability of pristine photoactive materials, for instance ITIC-derivatives, could be directly related to the stability of OSCs. As IT-4F exhibits excellent stability in electron-only devices,[4] we investigated the stability of three polymer donors in the same way in hole-only devices (indium tin oxide (ITO)/poly(3,4-ethylenedioxythiophene) polystyrene sulfonate (PEDOT:PSS)/polymer donor/MoOx/Ag) under illumination provided by white LEDs (spectra shown in Figure S1, Supporting Information). The devices were kept under dry nitrogen with oxygen and water level below 0.5 ppm. No obvious degradation was observed after ≈70 h illumination as shown in Figure 1c. Under extended illumination up to ≈360 h (relevant to significant performance degradation of OSCs discussed later), both PBDB-T and PM6 based hole-only devices showed minor changes as shown in Figure S2 (Supporting Information). These results demonstrate excellent intrinsic photostability of all polymers under measured condition relevant to the solar cells stability test.

Device stability under continuous LED illumination for optimized devices based on three different polymers is shown in **Figure 2.** First of all, all devices showed rather stabilized J_{SC} and V_{OC}. The degradation in PCE is mainly from FF losses, which is significantly different from fullerene-based devices, for which J_{SC} and V_{OC} losses are normally observed.[8,9] All three groups of devices showed burn-in losses in FF. Unlike the stabilized FF for PBDB-T-based devices, FF continuously decreased and remained only ≈80% after ≈1400 h illumination for both PM6- and PM7-based devices. This result is consistent with the previously reported degradation trend.[26] T_{80} lifetime for PM6- and PM7-based solar cells were estimated to be less than 1300 h, which is significantly reduced compared to that of PBDB-T-based devices (over 11 000 h).[4]

As PM6 and PM7-based solar cells exhibited very similar degradation behavior under illumination, we selected PM6:IT-4F for further systematic investigation. In general, for highly efficient organic photovoltaics (OPV) material systems, geminate recombination (recombination of bound electron–hole pairs) is significantly reduced and FF is the competition between bimolecular recombination and charge extraction.[28,30] To gain deeper insight into the charge recombination changes due to aging, charge carrier lifetime (measured by transient photovoltage, Figure S3, Supporting Information) as a function of charge carrier density (from charge extraction, Figure S3, Supporting Information) for fresh and aged PM6:IT-4F was investigated (**Figure 3**a). The recombination order (R) increased from ≈2 for fresh devices to 2.7 for aged devices. Increased recombination order in OSCs has been linked to trap-mediated recombination[31–34] and/or reduced mobility.[35] The mobility measured by photoinduced charge carrier extraction by linearly increasing voltage (Photo-CELIV) decreased from 1.1×10^{-4} cm^2 V^{-1} s^{-1} for fresh cells to 6.1×10^{-5} cm^2 V^{-1} s^{-1} for aged devices. Meanwhile, more dispersive transport was observed as shown in the delay-time variated Photo-CELIV (Figure 3b; and Figures S4 and S5, Supporting Information), which indicates existence of trapped charge carriers. To distinguish electron and hole mobility
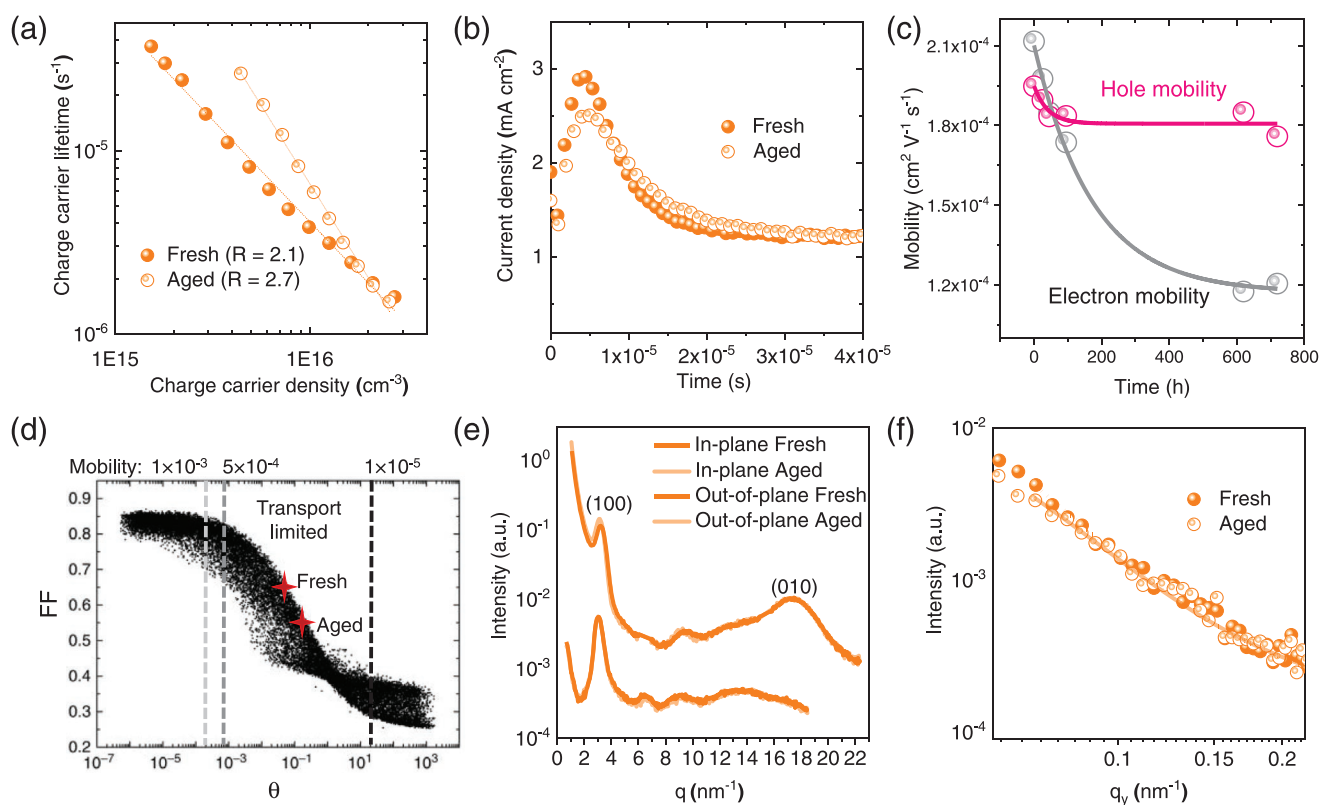
Figure 3. Transport and morphology investigation of PM6:IT-4F before and after aging test. a) Charge carrier lifetime as a function of charge carrier density. Recombination order (R) is indicated in the legend. b) Photo-CELIV with delay time of 1 μs. c) Electron and hole mobility measured as function of illumination time for electron-only and hole-only devices, respectively. Solid lines are single exponential decay fit of the experimental data. d) FF as a function of θ (figure of merit for competition between charge carrier extraction and recombination) calculated according to ref. [28]. Here the data points calculated from PM6:IT-4F were marked as 4-point-stars. The vertical dot lines indicate θ calculated from assumed mobility of 1×10^{-3} cm^2 V^{-1} s^{-1}, 5×10^{-4} cm^2 V^{-1} s^{-1}, and 1×10^{-5} cm^2 V^{-1} s^{-1} with other parameters keeping the same as for fresh PM6:IT-4F solar cells. e) In-plane and out-of-plane GIWAXS line cuts. f) GISAXS profiles (solid and open sphere: experiment data) and fit (solid and dot line) using Schulz–Zimm/DAB model.[29]

changes due to aging, electron-only (ITO/ZnO/AL/Ca/Al) and hole-only (ITO/PEDOT:PSS/AL/MoOx/Ag) devices were fabricated and their stability were measured under the same condition as for solar cells. The time-dependent J–V curves were shown in Figure S6 (Supporting Information), with extracted electron and hole mobility after different aging time shown in Figure 3c; and Table S2 (Supporting Information). Hole mobility remained relatively constant after a fast degradation to ≈95% of its initial value within ≈100 h. In contrast, electron mobility showed a continuous degradation to only ≈50% of its initial value after ≈600 h illumination. The FF degradation originates most probably from the decreased and increasingly unbalanced electron and hole mobility, especially in the weak electric field condition close to open-circuit. The same trend of J–V curves (Figure 2a–c) evolution has been reproduced in analytical simulations by solely decreasing mobility.[35] Bartesaghi et al. have developed a semiquantitative expressions of FF dependence on a figure of merit θ, which quantifies the ratio of recombination and extraction based on device and materials parameters including recombination rate, generation rate, film thickness, charge carrier mobility as well as internal voltage.[28] θ of the fresh and aged solar cells based on PM6:IT-4F was calculated and correlated with FF (Figure 3d; and Table S3, Supporting Information). By comparing with θ obtained by solely

varying mobility, it is obvious that the solar cells investigated here are limited by charge carrier mobility. Decreasing charge carrier mobility significantly reduced FF.

Mobility changes might originate from morphological traps[36] or chemical defects.[37] Here, we can exclude the chemical defects due to oxygen and water as well as intrinsic materials photostability issues. Grazing-incidence wide-angle X-ray scattering (GIWAXS) measurements were performed in order to gain deeper insights into morphological changes for PM6:IT-4F before and after aging under illumination, as shown in Figure 3; and Figures S7–S9 (Supporting Information). By comparing with the GIWAXS patterns of pristine polymer and IT-4F films, it is clear that polymer formed domains with high crystallinity (strong (100) diffraction and higher order diffraction peaks), while IT-4F domains are relatively less ordered (broad and weak diffraction intensity). After light aging, no significant difference was observed in GIWAXS in-plane direction. In out-of-plane direction, (100) peak at $q \approx 3.2$ nm^{-1} (from polymer crystals with edge-on orientation) showed a slight shift to a lower $q \approx 3.1$ nm^{-1} with only minor increase in intensity. Overall GIWAXS measured before and after aging did not significantly change. The stable crystalline polymer domains correlate well with relatively stable hole mobility.[38] A continuous decrease of electron mobility indicates more changes in

**ADVANCED
SCIENCE NEWS**

www.advancedsciencenews.com

**ADVANCED
MATERIALS**

www.advmat.de

the acceptor-related domains, including acceptor-rich domains and the amorphous mixed region. Grazing-incidence small-angle X-ray scattering (GISAXS) measurements were further performed as shown in Figure 3f; and Figure S10 (Supporting Information). A decreased slope in the range < 0.1 nm^{-1} was observed for aged films. Fitting with Schulz–Zimm/Debye–Anderson–Brumberger (DAB) model[29] revealed a slightly decreased correlation length (average spacing between different domains) from 18.9 ± 0.7 nm for the fresh film to 17.9 ± 0.7 nm after aging. However, the changes in the correlation length are in the same range with the error bar. These minor changes in GISAXS profiles but significant FF losses indicate that the underlying morphological changes are in a small scale in the mixed region which do not change the scattering contrast in GISAXS measurement but still play a significant role for electron transport.

Morphology for NFA systems is to a large extent governed by complex interplay among crystallization, diffusion, and demixing of the components, which is strongly materials-dependent.[39] In the PM6:IT-4F blend, the initial morphology formation is dominated by polymer aggregation/crystallization.[26] To evaluate the morphology evolution in the mixed region, miscibility between the three polymers with IT-4F was estimated by comparing the surface energy of each plain film as shown in Figure S11 and Table S4 (Supporting Information). The much higher surface energy of IT-4F (≈39 mN m^{-1}) compared to all three polymers (≈26 mN m^{-1}) indicates that in each polymer:IT-4F blend, demixing is thermodynamically favorable, which is consistent with the extremely low thermodynamic equilibrium compositions of IT-4F (weight percentage ≈7%) when blended with PM6 as reported by Ye et al.[40] It is also important to note that for strongly immiscible components, in order to optimize the device performance, it is critical to kinetically quench the composition away from the thermodynamic equilibrium state for adequate percolation. For the investigated system, the percolation limit of the acceptors was reported to be ≈20% (weight percentage).[40] Following the trend observed for fullerene-based systems, incompatibility between donor and acceptor normally leads to phase separation even under dark, and significantly reduces interface areas and then J_{SC}.[8] However, the incompatibility between PM6 and IT-4F is significantly influencing FF rather than J_{SC}, which is in stark contrast compared to previously reported fullerene-based systems.[9,18] To understand these differences, it should be noted that NFAs, as anisotropic small molecules, showed several orders of magnitude lower diffusion coefficient than those of isotropic fullerene derivatives.[39,41,42] One hypothesis is that in the mixed regions, due to reorganization of polymer chains and diffusion-limited NFA aggregation, small-scale isolated IT-4F domains below the percolation threshold are formed.[43] These small scale isolated IT-4F domains might broaden the density of states and reduce electron mobility under weak electric field, which mainly affects FF.[35]

Morphological related instability is expected to be largely dependent on the initial active-layer nanostructure. The effect of initial morphology changes by removing 1,8-diiodooctane (DIO) as a processing additive on the light stability were further investigated for devices based on PM6:IT-4F and PM7:IT-4F. Removing DIO from solvent processing leads to more disordered domains according to literature.[44] In this work, UV–vis spectra (**Figure 4**a) and GIWAXS (Figure S9, Supporting Information) proved that the ordering of both polymer and aggregated IT-4F domains were reduced when processed without DIO as solvent additive. For devices with less ordered donor and acceptor domains, a lower FF and J_{SC} were observed (Table S1, Supporting Information). The low FF is mainly due to low charge carrier mobility (6.5×10^{-5} cm^2 V^{-1} s^{-1}). The higher V_{OC} (0.85 vs 0.79 V for PM6-based OSCs) is a result of the higher bandgap (Figure 4a) as well as a higher charge transfer states energy (electroluminescence spectra shown in Figure S12, Supporting Information) due to the less aggregated IT-4F domains. Photostability of PM6-based devices is shown in Figure 4b,c. A much faster decay in FF was observed (below 80% after 150 h), which was also accompanied by similar amount of drop in J_{SC}. This trend is consistent in both cases of PM6 and PM7-based devices (Figure S13, Supporting Information). The results further confirm that the degradation in FF is rather morphology-related.

A detailed recombination/transport and morphology analysis on PM6-based devices before and after aging were performed. It is noted that the initial morphology changes from more to less ordered domains do not change the recombination behavior as ideal bimolecular recombination for the fresh solar cells (Figure 4d; and Figure S14, Supporting Information). The higher recombination order of 3 after aging was again linked to strongly increased trap-assisted recombination and/or reduced mobility.[34] Photo-CELIV indicated significant losses of charge carriers within 1 μs. The traps were also evidenced in Photo-CELIV (Figure 4e; and Figure S15, Supporting Information) as long lived charge carriers. Mott–Schottky analysis[45] of the impedance spectra (Figure 4f) showed significantly increased trap density to 5×10^{-16} cm^{-3} for aged solar cells. Increased sub-bandgap absorption was observed in sensitive photocurrent spectroscopy (Figure S16, Supporting Information). No significant changes were observed in GIWAXS and GISAXS measurement after aging (Figure 4g,h; and Figures S17 and S18), which is similar to devices processed with DIO. It is noted that the difference in initial film morphology significantly influences degradation rate. Devices with less ordered polymer and NFA aggregates showed much faster accumulation of trap states and correspondingly faster decrease in both FF and J_{SC}.

Improving ordering of donor and acceptor domains are believed to suppress the structural instability. In addition, this structural instability and resulted electron traps most probably happen in the amorphous mixed regions with formation of local isolated domains. To investigate the local structural instability, we further tested the stability of solar cells with macroscopically large acceptor components (D:A weight ratio of 1:4, statistics of photovoltaic parameters in Figure S19, Supporting Information). Donor and acceptor aggregations/ordering were modulated by thermal stress (from room temperature up to 200 °C) on the active layer before the deposition of top electrode. The initial morphology differences significantly influenced the photostability of the respective devices as shown in Figures S20 and S21 (Supporting Information). Decay rate was extracted by fitting the FF stability curves using single exponential decay fitting (exp($-t/\tau$), decay rate: $1/\tau$, Figure S21, Supporting Information). Optical bandgap determined from Tauc
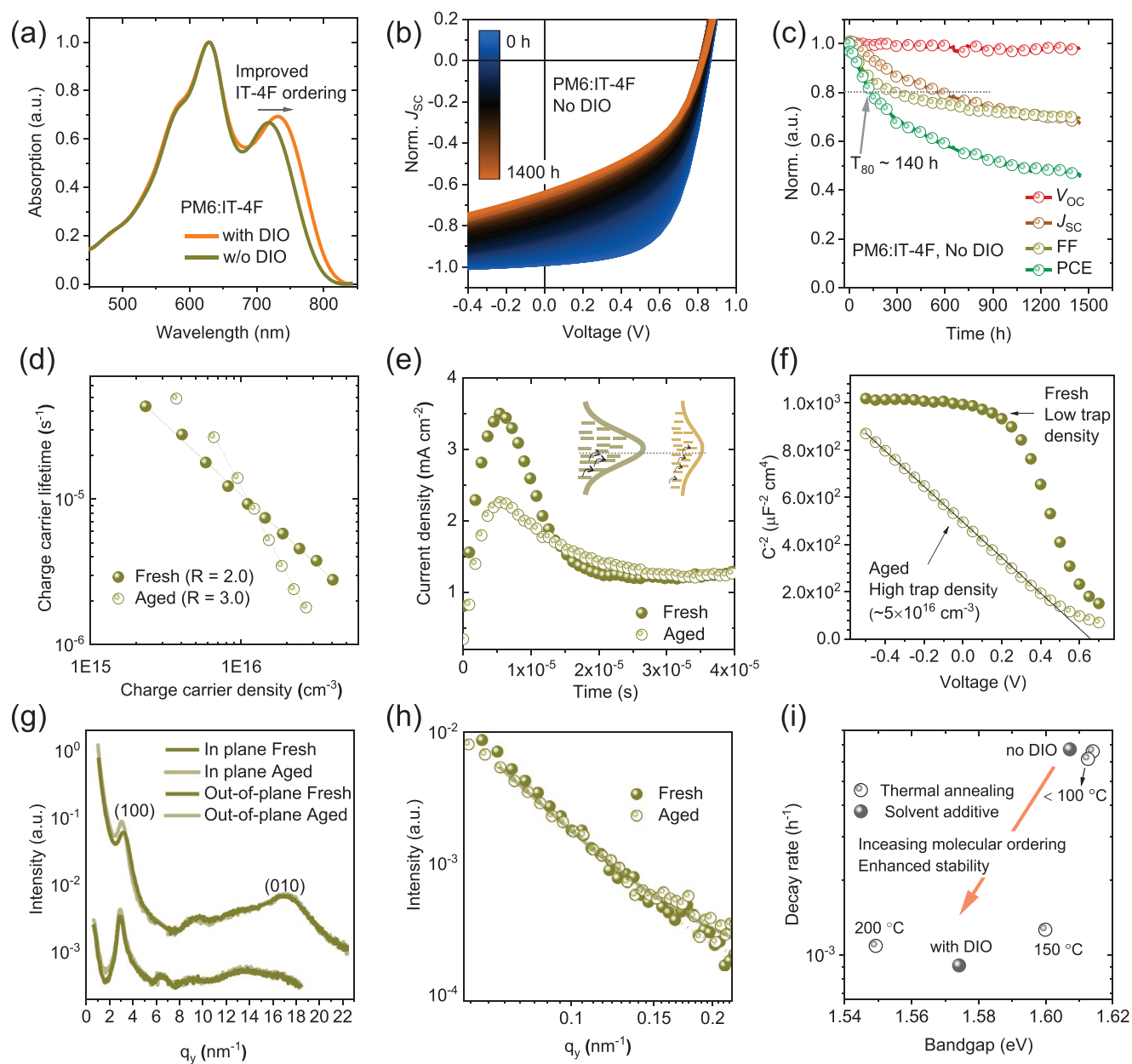
Figure 4. a) UV–vis absorption spectra of PM6:IT-4F films processed with or without DIO as solvent additive. b) Recorded current–voltage curves (with normalized initial short-circuit current density) and c) the evolution of photovoltaics parameters of devices with active layer processed without DIO as solvent additive. d) Charge carrier lifetime as a function of charge carrier density. Recombination order is indicated in the legend. e) Photo-CELIV with delay time of 1 µs. Inset shows the scheme of density of states before and after aging. Short lines are indications of discrete molecular energy levels. Arrows showed the hoping of trapped charge carriers to the transport level (gray dot line). f) Mott–Schottky plots (C^{-2}–V) of solar cells in the dark. Trap density for aged solar cells was extracted from the fitting (black dot line) of the experimental results. g) In-plane and out-of-plane GIWAXS line cut. h) GISAXS profiles (solid and open sphere: experiment data) and fit (solid and dot line) using Schulz–Zimm/DAB model.[29] Correlation length extracted from GISAXS fits for $q_y > 0.06$ nm^{-1} using SASfit is 21.5 ± 1.9 nm for fresh film and 20.5 ± 0.9 nm for aged film. i) FF decay rate as a function of the active-layer bandgap for solar cells based on PM6:IT-4F active layer processed under different conditions: D:A ratio 1:1 and processed with or without DIO with active layer annealed at 100 °C, or D:A ratio 1:4 with active layer annealed at different temperature.

plot of the film absorption spectra (Figure S22, Supporting Information) was used as an indicator for molecular ordering of IT-4F. For active layers without and with 100 °C annealing for 10 min, both FF and J_{SC} decreased in a relatively high rate. Preannealing active layers at 150 and 200 °C can significantly slow down FF and J_{SC} decay. These results indicate

that improving molecular ordering of the blend by thermal annealing can also improve morphological stability. It is noted that for devices annealed at 150 °C, which only showed local molecular reorganization (small changes in the absorption onset and microstructure (Figures S23 and S24, Supporting Information)) for better charge transport (increased FF, Figure S19,
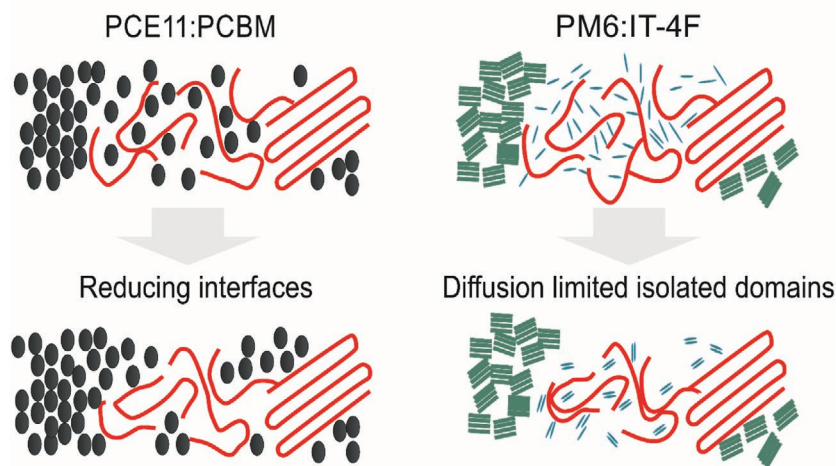
Scheme 1. Schematic representation of morphology changes of the mixed region for previously reported PCE11:PCBM system[8,18] (under dark or light) and the polymer:IT-4F systems under illumination. Due to diffusion of PCBM out of the polymer matrix, demixing in the amorphous regions for PCE11:PCBM system reduces D/A interfaces and hence photocurrent generation. In PM6:IT-4F mixed regions, small-scale isolated NFA domains might formed as a result of polymer aggregation/reorganization and low diffusion coefficient of IT-4F. These isolated domains act as morphological traps for electron transport and cause long-term FF degradation.

Supporting Information), the stability is significantly enhanced. Thus, it can be concluded that if the electron percolation is guaranteed, increasing the ordering of IT-4F can effectively suppress local structural instability. Thermal stability of the solar cells prepared under optimized condition was also tested (Figures S25 and S26, Supporting Information). At 65 °C, all devices are stable within 60 h. When tested under 85 °C, all OSCs showed FF dominated performance losses. In addition, the thermal stability of PM6-based OSCs showed a degradation rate depending on initial morphology as has been observed under illumination, i.e., improving molecular ordering can slow down the FF losses. These results indicate that degradation under light- and thermal-stress originates from the same morphological instability. It is noted that the degradation rate is different under light and thermal stress, which depends on many factors, e.g., temperature, light intensity and so on.

Fullerene derivative- (e.g., PCE11:PCBM[8]) and NFA-based systems exhibit distinct microstructure degradation mechanisms as we schematically illustrated in **Scheme 1**. We used a simplified three-phase model for comparison: crystalline polymer domains, ordered aggregated acceptor domains, as well as mixed region with disordered acceptors and randomly distributed polymer chains. For PCE11:PCBM domains, the mixed regions undergo demixing even at room temperature in the dark due to diffusion of PCBM out of the polymer matrix. This demixing leads to serious J_{SC} losses due to reduced D:A interfaces as well as moderate FF losses due to break down of percolation threshold.[8,39,46] While in NFA systems studied here, due to low NFA diffusion,[43] aggregation/reorganization of polymers and acceptors only lead to local crystallization/aggregation of NFAs in a small scale. These small aggregates in the amorphous domains significantly reduced electron

percolation, broadened density of states, and increased electron trapping probability, which finally lead to long-term losses in FF. Depending on the mobility, J_{SC} can also be influenced to different extent. The influence from these local NFA aggregation significantly depends on the preordering of NFAs in mixed regions. For films featuring initially disordered NFAs with composition far away from the thermodynamic equilibrium in the mixed region, aggregation/reorganization of both polymers and NFAs as well as low diffusion of acceptors leads to morphological traps, which result in severe charge trapping and recombination losses. The morphological changes mainly reduce FF, while J_{SC} can also be affected when severe traps are formed. Depending on the interplay between the initial morphology in the mixed region, the materials compatibility and the diffusion of NFAs, this morphological changes can either cause burn-in losses of FF in a short-term or a long-term continuous degradation. Considering that low molecular diffusion coefficient is a common feature for NFAs, we believe that the morphological-related instability observed here can be relevant in general for FF losses in many reported NFA-based OSCs, for instance IDTBR[11] and ITIC-derivatives.[4]

In summary, photostability and degradation mechanisms of OSCs based on PBDB-T derivatives as electron donors and IT-4F as electron acceptor were systematically investigated. While PBDB-T-based devices were stabilized after burn-in losses, both PM6 and PM7-based devices showed continuous degradation in FF, leading to significantly reduced operational lifetime. Excellent light stability of the hole-only devices based on the polymers ruled out intrinsic photoinstability as a potential mechanism. Degradation rate of PM6- and PM7-based devices was strongly related to the initial thin film morphology. Increasing molecular ordering by solvent additives or thermal stress could significantly increase morphological and device photostability. In contrary to reduced interfaces in PCE11:PCBM-based systems due to diffusion and agglomeration of PCBM out of polymer matrix, diffusion of IT-4F was strongly restricted within the polymer matrix, which most probably leads to small scale isolated domains as morphological traps. In order to achieve stable and high-performance organic solar cells under illumination, it is essential to engineer the mixed regions from both thin film formation kinetics and materials intrinsic properties, e.g., materials compatibility and NFA diffusion constant.

In order to accelerate the development of OSCs with both high performance and stability, a fast and reliable way of screening materials with high stability is in high demand. We propose a guideline for screening materials with high stability in the following aspects: 1) IV measurement of single carrier devices based on either donor or acceptor [4] thin films under different aging conditions can give a fast and reliable evaluation of the materials' intrinsic photo- and/or thermal-stability.

**ADVANCED
SCIENCE NEWS**

www.advancedsciencenews.com

**ADVANCED
MATERIALS**

www.advmat.de

2) Device structure has to be both chemically and mechanically robust in order to fully exclude the potential degradation induced by interface layers. Changing initial thin film morphology and comparing the degradation rate can also help to distinguish morphological and interface instability. 3) To speed up the screening speed, increased levels of stress can be utilized for both OSCs and single carrier devices, e.g., concentrated light, thermal stress at elevated temperature, light plus heat, environmental conditions including water and oxygen, and so on.

Supporting Information

Supporting Information is available from the Wiley Online Library or from the author.

Conflict of Interest

The authors declare no conflict of interest.

[1] C. Yan, S. Barlow, Z. Wang, H. Yan, A. K. Y. Jen, S. R. Marder, X. Zhan, *Nat. Rev. Mater.* **2018**, *3*, 18003.

[2] M. A. Green, E. D. Dunlop, D. H. Levi, J. Hohl-Ebinger, M. Yoshita, A. W. Y. Ho-Baillie, *Prog. Photovoltaics* **2019**, *27*, 565.

[3] N. Li, I. McCulloch, C. J. Brabec, *Energy Environ. Sci.* **2018**, *11*, 1355.

[4] X. Du, T. Heumueller, W. Gruber, A. Classen, T. Unruh, N. Li, C. J. Brabec, *Joule* **2019**, *3*, 215.

[5] E. M. Speller, A. J. Clarke, J. Luke, H. K. H. Lee, J. R. Durrant, N. Li, T. Wang, H. C. Wong, J.-S. Kim, W. C. Tsoi, Z. Li, *J. Mater. Chem. A* **2019**, *7*, 23361.

[6] E. M. Speller, A. J. Clarke, N. Aristidou, M. F. Wyatt, L. Francàs, G. Fish, H. Cha, H. K. H. Lee, J. Luke, A. Wadsworth, A. D. Evans, I. McCulloch, J.-S. Kim, S. A. Haque, J. R. Durrant, S. D. Dimitrov, W. C. Tsoi, Z. Li, *ACS Energy Lett.* **2019**, *4*, 846.

[7] P. Cheng, X. Zhan, *Chem. Soc. Rev.* **2016**, *45*, 2544.

[8] N. Li, J. D. Perea, T. Kassar, M. Richter, T. Heumueller, G. J. Matt, Y. Hou, N. S. Guldal, H. Chen, S. Chen, S. Langner, M. Berlinghof, T. Unruh, C. J. Brabec, *Nat. Commun.* **2017**, *8*, 14541.

[9] C. Zhang, T. Heumueller, W. Gruber, O. Almora, X. Du, L. Ying, J. Chen, T. Unruh, Y. Cao, N. Li, C. J. Brabec, *ACS Appl. Mater. Interfaces* **2019**, *11*, 18555.

[10] W. R. Mateker, M. D. McGehee, *Adv. Mater.* **2017**, *29*, 1603940.

[11] N. Gasparini, M. Salvador, S. Strohm, T. Heumueller, I. Levchuk, A. Wadsworth, J. H. Bannock, J. C. de Mello, H. J. Egelhaaf, D. Baran, I. McCulloch, C. J. Brabec, *Adv. Energy Mater.* **2017**, *7*, 1700770.

[12] J. Xiao, M. Ren, G. Zhang, J. Wang, D. Zhang, L. Liu, N. Li, C. J. Brabec, H.-L. Yip, Y. Cao, *Sol. RRL* **2019**, *3*, 1900077.

[13] X. Xu, J. Xiao, G. Zhang, L. Wei, X. Jiao, H.-L. Yip, Y. Cao, *Sci. Bull.* **2019**, *65*, 208.

[14] H. Cha, J. Wu, A. Wadsworth, J. Nagitta, S. Limbu, S. Pont, Z. Li, J. Searle, M. F. Wyatt, D. Baran, J. S. Kim, I. McCulloch, J. R. Durrant, *Adv. Mater.* **2017**, *29*, 1701156.

[15] Y. He, T. Heumüller, W. Lai, G. Feng, A. Classen, X. Du, C. Liu, W. Li, N. Li, C. J. Brabec, *Adv. Energy Mater.* **2019**, *9*, 1900409.

[16] Y. Lin, J. Wang, Z. G. Zhang, H. Bai, Y. Li, D. Zhu, X. Zhan, *Adv. Mater.* **2015**, *27*, 1170.

[17] N. Y. Doumon, M. V. Dryzhov, F. V. Houard, V. M. Le Corre, A. Rahimi Chatri, P. Christodoulis, L. J. A. Koster, *ACS Appl. Mater. Interfaces* **2019**, *11*, 8310.

[18] C. Zhang, T. Heumueller, S. Leon, W. Gruber, K. Burlafinger, X. Tang, J. D. Perea, I. Wabra, A. Hirsch, T. Unruh, N. Li, C. J. Brabec, *Energy Environ. Sci.* **2019**, *12*, 1078.

[19] C. J. Schaffer, C. M. Palumbiny, M. A. Niedermeier, C. Jendrzejewski, G. Santoro, S. V. Roth, P. Muller-Buschbaum, *Adv. Mater.* **2013**, *25*, 6760.

[20] J. D. Perea, S. Langner, M. Salvador, B. Sanchez-Lengeling, N. Li, C. Zhang, G. Jarvas, J. Kontos, A. Dallos, A. Aspuru-Guzik, C. J. Brabec, *J. Phys. Chem. C* **2017**, *121*, 18153.

[21] A. Distler, T. Sauermann, H.-J. Egelhaaf, S. Rodman, D. Waller, K.-S. Cheon, M. Lee, D. M. Guldi, *Adv. Energy Mater.* **2014**, *4*, 1300693.

[22] T. Heumueller, W. R. Mateker, A. Distler, U. F. Fritze, R. Cheacharoen, W. H. Nguyen, M. Biele, M. Salvador, M. von Delius, H.-J. Egelhaaf, M. D. McGehee, C. J. Brabec, *Energy Environ. Sci.* **2016**, *9*, 247.

[23] T. Heumueller, W. R. Mateker, I. T. Sachs-Quintana, K. Vandewal, J. A. Bartelt, T. M. Burke, T. Ameri, C. J. Brabec, M. D. McGehee, *Energy Environ. Sci.* **2014**, *7*, 2974.

[24] T. Heumueller, T. M. Burke, W. R. Mateker, I. T. Sachs-Quintana, K. Vandewal, C. J. Brabec, M. D. McGehee, *Adv. Energy Mater.* **2015**, *5*, 1500111.

[25] B. B. Fan, X. Y. Du, F. Liu, W. K. Zhong, L. Ying, R. H. Xie, X. F. Tang, K. An, J. M. Xin, N. Li, W. Ma, C. J. Brabec, F. Huang, Y. Cao, *Nat. Energy* **2018**, *3*, 1051.

[26] S. Zhang, Y. Qin, J. Zhu, J. Hou, *Adv. Mater.* **2018**, *30*, 1800868.

[27] Q. P. Fan, Q. L. Zhu, Z. Xu, W. Y. Su, J. Chen, J. N. Wu, X. Guo, W. Ma, M. J. Zhang, Y. F. Li, *Nano Energy* **2018**, *48*, 413.

[28] D. Bartesaghi, C. Perez Idel, J. Kniepert, S. Roland, M. Turbiez, D. Neher, L. J. Koster, *Nat. Commun.* **2015**, *6*, 7083.

**ADVANCED
SCIENCE NEWS**

www.advancedsciencenews.com

**ADVANCED
MATERIALS**

www.advmat.de

[29] T. L. Lin, U. Jeng, C. S. Tsao, W. J. Liu, T. Canteenwala, L. Y. Chiang, *J. Phys. Chem. B* **2004**, *108*, 14884.

[30] L. J. A. Koster, E. C. P. Smits, V. D. Mihailetchi, P. W. M. Blom, *Phys. Rev. B* **2005**, *72*, 085205.

[31] D. Rauh, C. Deibel, V. Dyakonov, *Adv. Funct. Mater.* **2012**, *22*, 3371.

[32] R. A. Street, *Phys. Rev. B* **2011**, *84*, 075208.

[33] A. Wagenpfahl, *J. Phys.: Condens. Matter* **2017**, *29*, 373001.

[34] C. Göhler, A. Wagenpfahl, C. Deibel, *Adv. Electron. Mater.* **2018**, *4*, 1700505.

[35] U. Wurfel, D. Neher, A. Spies, S. Albrecht, *Nat. Commun.* **2015**, *6*, 6951.

[36] R. C. I. MacKenzie, C. G. Shuttle, M. L. Chabinyc, J. Nelson, *Adv. Energy Mater.* **2012**, *2*, 662.

[37] J. Schafferhans, A. Baumann, C. Deibel, V. Dyakonov, *Appl. Phys. Lett.* **2008**, *93*, 093303.

[38] D. T. Scholes, P. Y. Yee, J. R. Lindemuth, H. Kang, J. Onorato, R. Ghosh, C. K. Luscombe, F. C. Spano, S. H. Tolbert, B. J. Schwartz, *Adv. Funct. Mater.* **2017**, *27*, 1702654.

[39] M. Ghasemi, H. Hu, Z. Peng, J. J. Rech, I. Angunawela, J. H. Carpenter, S. J. Stuard, A. Wadsworth, I. McCulloch, W. You, H. Ade, *Joule* **2019**, *3*, 1328.

[40] L. Ye, S. Li, X. Liu, S. Zhang, M. Ghasemi, Y. Xiong, J. Hou, H. Ade, *Joule* **2019**, *3*, 443.

[41] B. Watts, W. J. Belcher, L. Thomsen, H. Ade, P. C. Dastoor, *Macromolecules* **2009**, *42*, 8392.

[42] N. D. Treat, M. A. Brady, G. Smith, M. F. Toney, E. J. Kramer, C. J. Hawker, M. L. Chabinyc, *Adv. Energy Mater.* **2011**, *1*, 82.

[43] L. Yu, D. Qian, S. Marina, F. A. A. Nugroho, A. Sharma, S. Hultmark, A. I. Hofmann, R. Kroon, J. Benduhn, D. M. Smilgies, K. Vandewal, M. R. Andersson, C. Langhammer, J. Martin, F. Gao, C. Muller, *ACS Appl. Mater. Interfaces* **2019**, *11*, 21766.

[44] H. Chen, J. Qu, L. Liu, W. Chen, F. He, *J. Phys. Chem. Lett.* **2019**, *10*, 936.

[45] O. Almora, M. Garcia-Batlle, G. Garcia-Belmonte, *J. Phys. Chem. Lett.* **2019**, *10*, 3661.

[46] Z. Peng, X. Jiao, L. Ye, S. Li, J. J. Rech, W. You, J. Hou, H. Ade, *Chem. Mater.* **2018**, *30*, 3943.

1908305 (9 of 9)